Mechanical properties and formability of metal–polymer–metal sandwich composites

Mechanical properties and formability of metal-polymer-metal sandwich composites

Archimede Forcellese[1] and Michela Simoncini[2*]

[1]*Università Politecnica delle Marche, DIISM, Via Brecce Bianche, 60121 Ancona, Italy;*

a.forcellese@univpm.it - http://orcid.org/0000-0003-1380-4596

[2]*Università degli Studi eCampus, via Isimbardi 10, 22060 Novedrate (CO); Italy*

**Corresponding author: m.simoncini@staff.univpm.it; michela.simoncini@uniecampus.it*

https://orcid.org/0000-0001-5356-9012

ABSTRACT

Mechanical properties and formability of a three layers metal-polymer-metal sandwich composite were studied as a function of the angle of the sample axis with respect to the rolling direction. Sandwich was obtained by bonding a polymer core, 0.4 mm in thickness, between two steel sheets, each of them with a thickness of 0.2 mm. The strength-deformation characteristics and anisotropic behavior were investigated by performing uniaxial tensile tests. Hemispherical punch tests were also carried out in order to evaluate both formability, in terms of limiting dome height and forming limit curves, and thinning attitude of the metal-polymer-metal sandwich composite. Finally, the fracture surfaces of both tensile and hemispherical punch-formed samples were analyzed by means of the scanning electron microscopy. It was observed that the samples oriented at 45° to rolling direction are characterized by the highest mechanical properties and formability as compared to the ones at 0° and 90°. Such results were related to the debonding mechanism occurring at the interfaces between steel sheet and plastic core as the angle of the sample axis was 0° and 90°.

Keyword: metal-polymer-metal sandwich composite; mechanical properties; anisotropy; formability; thinning; SEM fractography.

1. INTRODUCTION

An emerging need in the field of lightweight structures [1–3] is the availability of sheet panels able to combine the advantages offered by different materials, such as high specific strength and high specific stiffness [4], high bending strength [5], high vibrational and thermal resistances [6,7], and high impact-energy absorption [8,9]. To this purpose, sandwich composites, consisting of two thin-high strength metal skins and a polymer core, can provide an innovative alternative to monolithic metal sheets. By combining polymers and metals, low weight and high strength and stiffness multi-layer structures can be obtained [4,10,11]. Furthermore, the metal-polymer-metal (MPM) sandwich composites are characterized by high deformation potential that makes them suitable to be formed in complex shapes. Kim et al. [12] have shown that AA5182/polypropylene/AA5182 sandwich panels, characterized by formability and strain rate sensitivity higher than those exhibited by the aluminum sheet, allows the obtaining of complex structures for automotive applications.

Since the mechanical properties and formability of metals significantly differ from those of polymers, the MPM sandwich structures are characterized by different properties with respect to constituent materials. To this purpose, Harhash et al. [13] have shown that the strain hardening exponent and strength coefficient of 316L/polypropylene–polyethylene/316L sandwich decrease as compared to the ones measured on the monolithic steel sheet due to the contribution of the soft core on the strengthening behavior of the MPM sandwich.

Notwithstanding several studies are available in the scientific literature on formability of monolithic metal sheets [14–19], few researches on forming attitude of MPM sandwich composites have been undertaken. Forming processes of parts in MPM sandwich usually involve issues, such as wrinkling, delamination and shearing, related to the inadequate interlayer metal-polymer adhesion. The adhesive strength at the metal-polymer interfaces is a key factor for MPM sandwich composites since the interfacial interaction generates a system that can strongly affect the sheets to either act independently, weakly or as strongly coupled. A weak polymer core can act as a lubricant between the metal skins; such behavior can cause the occurrence of debonding at interfaces between sheet and plastic core, leading to a sliding of metal skins and a premature failure during forming operations. On the other hand, a too strong adhesion force between polymer core and metal sheet can negatively affect formability since the continuous smooth sliding between

layers is prevented [20,21]. Furthermore, as reported by Kim and Yu in [22], the bonding between dissimilar materials to obtain a multi-layer component generates inhomogeneities leading to discontinuities in stress distributions across the sheet thickness. A further drawback taking place during forming processes of sandwich composites is the higher tendency to wrinkle with respect to the monolithic metal sheets. This is due to the weak interlayer adhesion that, allowing the two metal sheets to act independently, make them be more susceptible to wrinkling than a single thicker sheet. Also delamination can occur during forming operations due to the different lengths of the metal skins, as they are deformed around the die, that can cause the occurrence of high shear forces in the polymer core [20,23]. Harhash et al. [24] analyzed the effect of the polymer core thickness on springback of steel-polymer-steel sandwich composites; they showed a reduction in springback with decreasing core thickness even though, with thicker polymer films, crack probability rises due to the increase in tensile stresses on the outer metal skin. Furthermore, as shown by Carradò et al. [4], the presence of cavities in the polymer core, caused by air bubbles trapped during the manufacturing process of sandwich laminates, can accelerate cracking. Factors, such as the inhomogeneous cross-section structure of multi-layer sandwiches, composition and characteristics of the different constituents, bonding method used to hold together the single layers, shape complexity of the final component, forming technique as well as loading conditions, can strongly affect the success of forming processes of multi-layer materials and, consequently, the final performances of the formed parts.

In this framework, the present work aims at studying the deformation behavior of a three-layers sandwich composite obtained by assembling a polymer core film between two thin cover sheets in higher-strength interstitial free steel. In order to investigate the influence of fiber orientation on strength and ductility of MPM sandwich composite, uniaxial tensile tests were performed on samples with different angular orientations with respect to the rolling direction (RD) of the metal sheets. The values of normal and planar anisotropy were also calculated by performing interrupted tensile tests in the field of uniform deformation. Formability of metal-polymer-metal sandwich, in terms of both limiting dome height and forming limit curves, as a function of angular orientation with respect to RD, was evaluated by hemispherical punch test. The thinning attitude of MPM panels was also investigated by measuring thickness of each constituent layer along the radial cross-section of disk-shaped sample at different angular orientations and punch strokes. Finally,

the deformation behavior of MPM sandwich composite was related to the failure mode by SEM fractography.

2. MATERIAL AND EXPERIMENTAL PROCEDURES

2.1 Workpiece material

The three-layers MPM sandwich composite was obtained by bonding a core film in polypropylene polyethylene (PP-PE) resin, 0.4 mm in thickness, with two cover sheets in higher-strength interstitial free steel for cold forming (HX220Y), each of them 0.2 mm thick (Fig. 1). The manufacturing process consists of a two-stage roll bonding process. In the first stage, an adhesive layer, with a thickness of 10 μm, was applied on the steel sheet and cured at 260°C for its activation. Then, the polymer film was heated at 120°C and roll bonded to the steel sheet. In the second stage, the steel/polymer assembly was roll bonded with the second pre-treated steel sheet in order to obtain the whole sandwich.

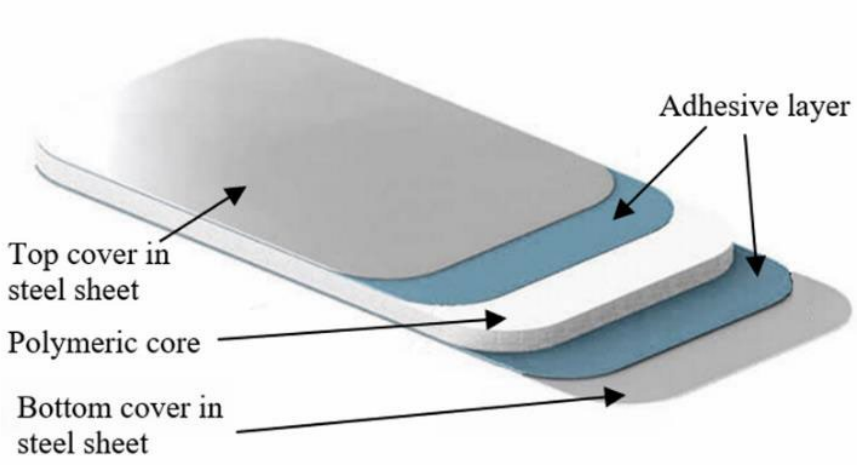

Fig. 1. Different layers of the metal-polymer-metal sandwich composite.

2.2 Experimental procedures

2.2.1 Uniaxial tensile tests

Strength and ductility of the MPM sandwich composite were evaluated by means of uniaxial tensile tests performed, according to ASTM E8/E8M and BS EN 895, on a servo-hydraulic testing machine (MTS 810®) equipped with a 250 kN load cell. A constant crosshead speed of 0.1 mm/s was imposed during tests carried out at room temperature. The instantaneous strain along the loading direction was measured using an extensometer clamped down on the sample (Fig. 2a). Fig. 2b shows a magnification of the polymer core between the two cover sheets in a fracture surface.

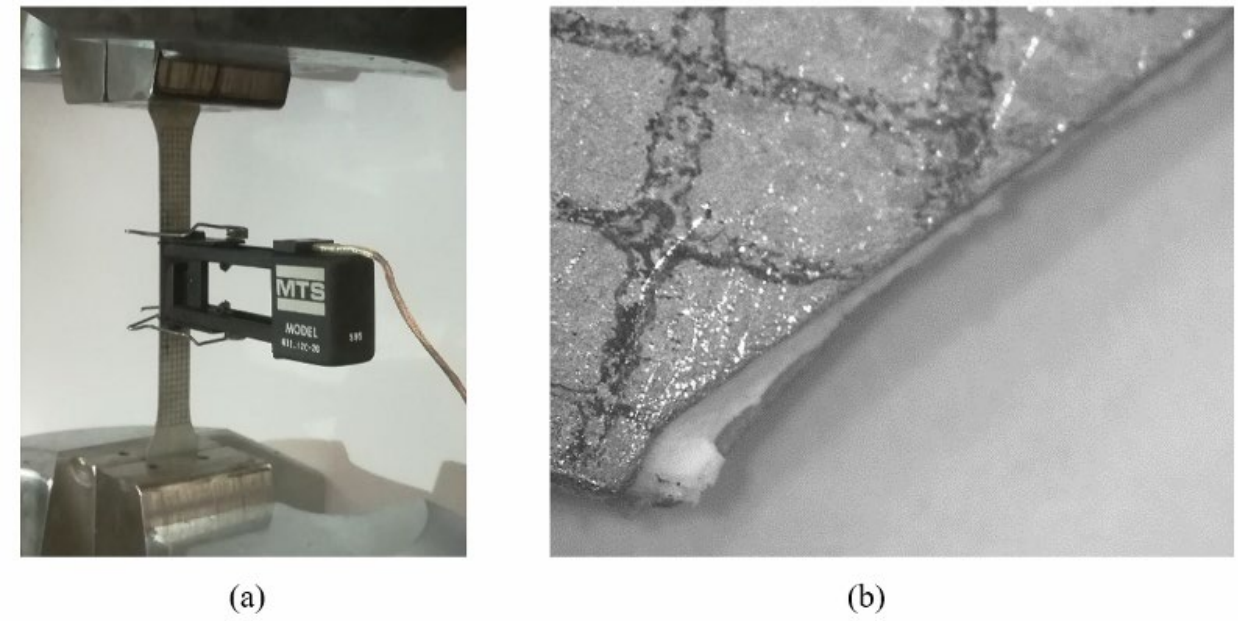

Fig. 2. (a) Tensile sample in metal-polymer-metal composite grasped by the machine head clamps and (b) typical fracture surface of a tensile sample.

Fig. 3 shows the tensile samples obtained by water jet cutting (WJC) with the loading axis oriented at 0°, 45° and 90° with respect to the rolling direction of the steel sheets.

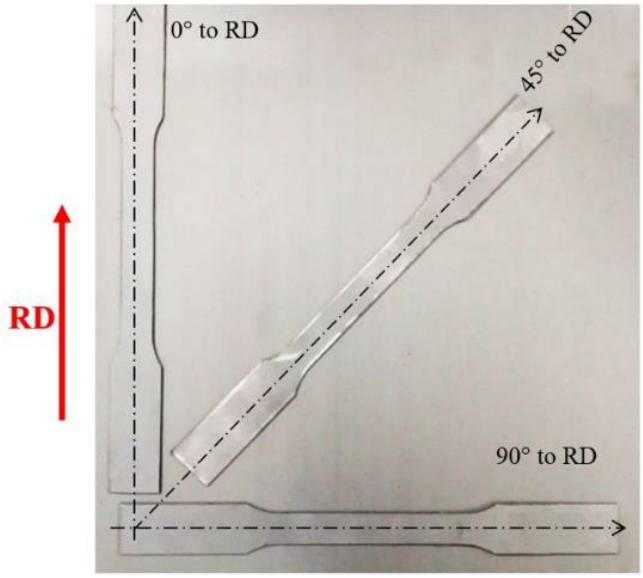

Fig. 3. Tensile samples obtained by WJC at different orientations to the rolling direction.

In addition, mechanical properties of the cover sheets in HX220Y steel, 0.2 mm in thickness, were investigated at 0°, 45° and 90° with respect to the RD.

The experimental results were plotted as nominal stress (s) vs. nominal strain (e). The elastic modulus (E), yield strength (YS), ultimate tensile strength (UTS), total uniform elongation in percentage (e_u) and ultimate elongation in percentage (e_t) were derived from the s-e curves. The values of true stress (σ) and true strain (ε), in the region of uniform plastic deformation, were calculated by means of the s-e data and processed to determine the strain hardening exponent (n) of the Ludwik-Hollomon's equation [25] according to the ASTM E646 standard guidelines [26]. Finally, the anisotropy was evaluated by interrupting tensile tests at an elongation value of 15% so that the plastic deformation was in the field of uniform deformation [25]. The normal anisotropy (R) was calculated as the ratio between true strain in the width direction (ε_w) and true strain in the thickness one (ε_t) of the sample:

$$R = \frac{\varepsilon_w}{\varepsilon_t} \quad (1)$$

The average normal anisotropy ($\overline{R}$) and the planar anisotropy (ΔR) were calculated according to the following relationships [25]:

$$\bar{R} = \frac{R_0 + R_{90} + 2 \cdot R_{45}}{4} \quad (2)$$

$$\Delta R = \frac{R_0 + R_{90} - 2 \cdot R_{45}}{4} \quad (3)$$

where the subscripts 0, 45 and 90 refer to the normal anisotropy obtained on tensile samples with angular orientations of 0°, 45° and 90° to the rolling direction.

The repeatability of results was assured by performing at least three tensile tests in each condition.

2.2.2 Hemispherical punch tests

Formability of the metal-polymer-metal sandwich composite was evaluated by means of the hemispherical punch tests performed, at room temperature, with constant crosshead speed equal to 0.1 mm/s, using a servo-hydraulic testing machine (MTS 810®). The tooling, shown in Fig. 4a, consists of a die, a tightening screw cap, a blank-holder with drawbeads, and a hemispherical punch with a diameter of 18 mm [27].

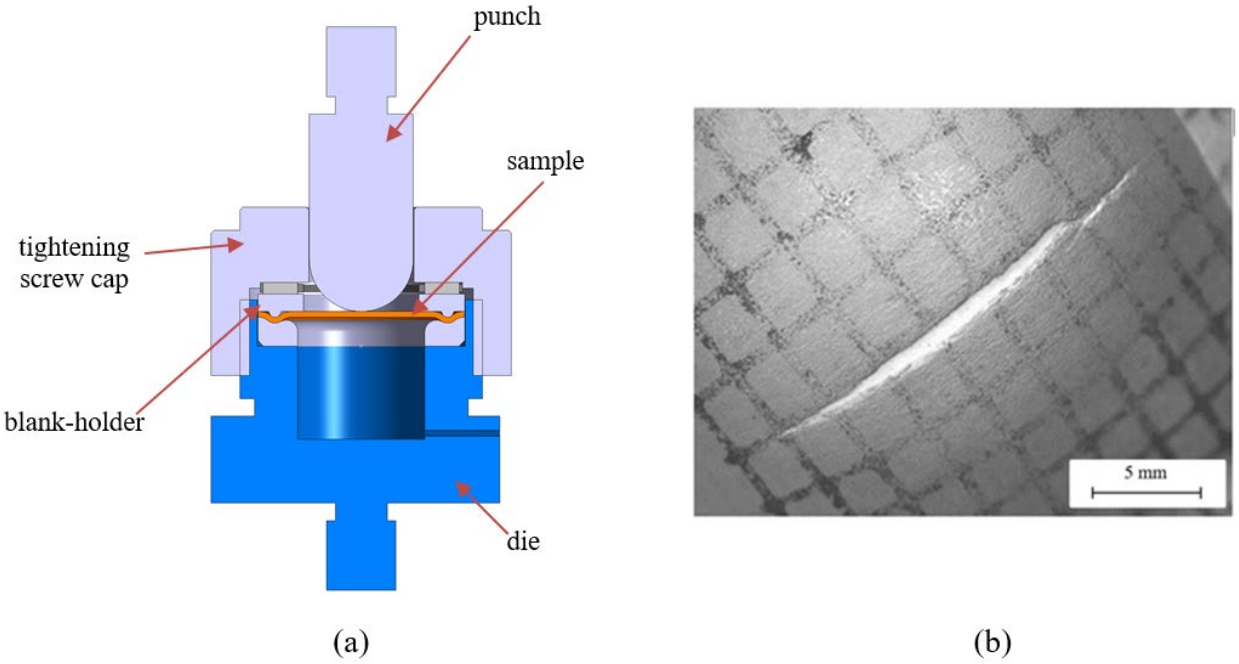

Fig. 4. (a) Tooling used in the hemispherical punch tests and (b) disk-shaped sample in metal-polymer-metal composite at the onset of failure.

In order to reduce friction, the hemispherical punch was lubricated using foils in polytetrafluoroethylene with diameter smaller than the punch one in order to prevent the foil wrinkling. Tests were carried out until the onset of failure (Fig. 4b).

The outputs of the hemispherical punch test were the limiting dome height (LDH) and forming limit curve (FLC).

The limiting dome height was defined as the stroke at the peak value of the punch load vs. punch stroke curve. It was obtained by carrying out the hemispherical punch test using a disk-shaped sample, with a diameter equal to 50 mm (Fig. 5), whose edges were rigidly clamped by the blankholder in order to prevent their inward motion during testing. Limiting dome height value of the cover sheets in HX220Y steel was also measured.

Forming limit curve provides a graphical representation of the forming behavior of sheet at the onset of failure in the space of principal strains (ε_1 and ε_2): a strain state falling above the FLC involves a local fracture in the workpiece whilst a safety condition occurs as ε_1 and ε_2 are characterized by values below the forming limit curve [28]. FLC was obtained by means of the hemispherical punch test using different sample geometries; they were characterized by an outer circular shape, 50 mm in diameter (D), and different values of remaining sample width (W), in order to obtain D/W ratios varying from 1 to 4 (Fig. 5), according to the EN ISO 12004-2 [28]. In order to evaluate the effect of angular orientation on the FLC of the MPM sandwich composite, samples were obtained by WJC at 0°, 45° and 90° to the rolling direction of steel sheets.

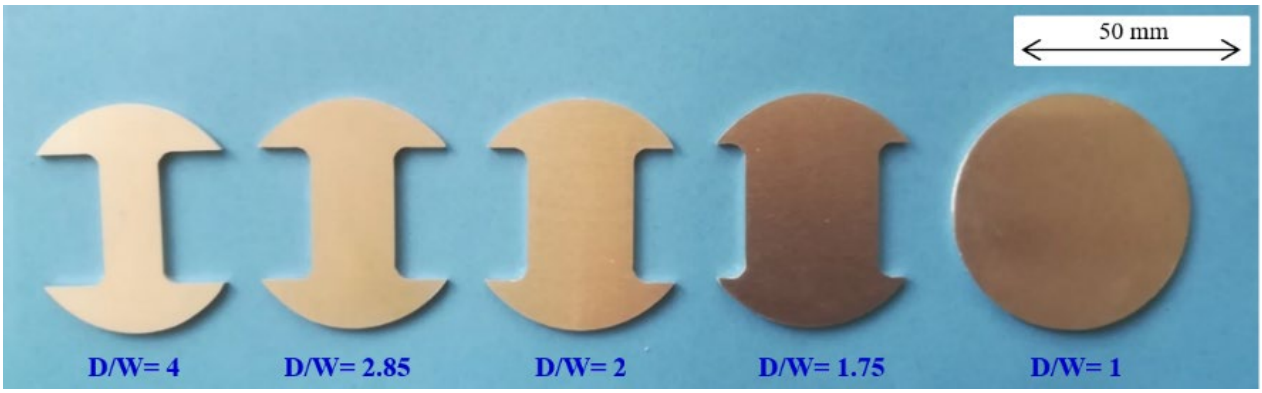

Fig. 5. Sample with different geometries used in the hemispherical punch tests to obtain the FLCs.

A regular square grid, with a side equal to 2 mm, was imprinted on the sample surface and acquired before testing by a couple of digital cameras. The system was also used to acquire the deformed grid after testing. An accurate optical grid method was used to measure the major (ε_1) and minor (ε_2) strains by the differentiation between the computed 3D coordinates of the grid corners after testing (Fig. 6) and the un-deformed ones before testing [27].

Finally, several hemispherical punch tests were performed on disk-shaped samples at punch stroke values equal to 5, 5.5 and 6 mm in order to investigate the effect of the punch stroke on the thickness variation of each layer of the MPM sandwich before the onset of necking.

At least three experiments were carried out for each test condition investigated.

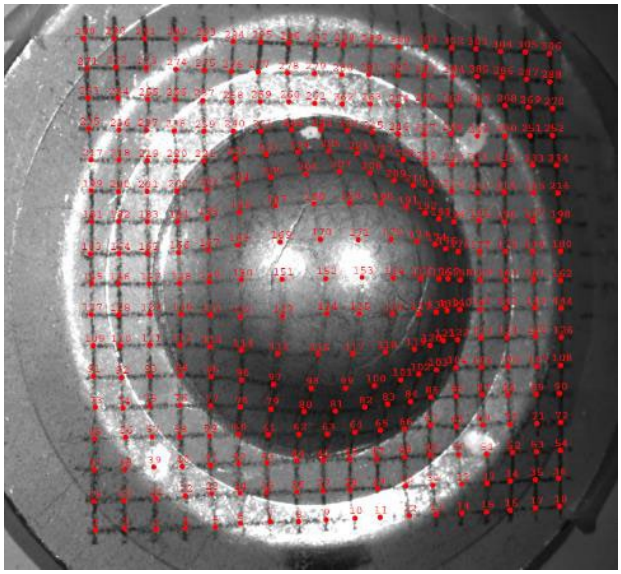

Fig. 6. Disk-shaped sample with the square grid after the 3D coordinates reconstruction by the stereoscopic algorithm.

2.2.3 Optical and scanning electron microscopies

The material flow and thickness variation during deformation of the three layers MPM sandwich composite were investigated as a function of the angular orientation with respect to the rolling direction. To this purpose, the disk-shaped samples deformed at fixed values of punch stroke of 5, 5.5 and 6 mm were cut along the radial cross-section at 0°, 45° and 90° to RD. Then, they were embedded and, after metallographic preparation, were analyzed using the optical microscope Leica DMi8 (Fig. 7). The thickness of each layer was measured using the image analysis system Leica

Application Suite and the thickness variation (Δt) was obtained by the difference between the measured thickness and the initial one.

Fig. 7. Disk-shaped sample cut along the radial cross-section at 0° with respect to RD and embedded for microstructural analysis.

High magnification images of the fracture surface of samples tested by tensile and hemispherical punch tests were acquired using the scanning electron microscope (SEM) Philips XL20. To this purpose, the fractured samples were coated by a metallization process in order to make conductive the polymer core.

3. RESULTS AND DISCUSSION

3.1 Tensile behavior

Fig. 8a shows typical s-e curves of the three-layers sandwich composite as a function of the angle of the tensile sample axis with respect to the rolling direction; fractured samples after tensile tests are shown in Fig.8b. In the elastic region, the nominal stress linearly increases with nominal strain until yielding with an average Young modulus equal to 79.2 GPa; then, the s value rises with a non-linear behavior up to a peak value corresponding to the onset of necking. The highest s value in the longitudinal and transverse directions (0° and 90°) is obtained at very similar strain levels

whilst, as the angle of the sample axis with respect to the rolling direction is equal to 45°, the peak value is reached at a higher strain. After necking, the nominal stress in the 0° and 90° directions does not exhibit an appreciable decrease with a further increase in strain until failure contrarily to the 45° direction at which a decay in the s value takes place before failure.

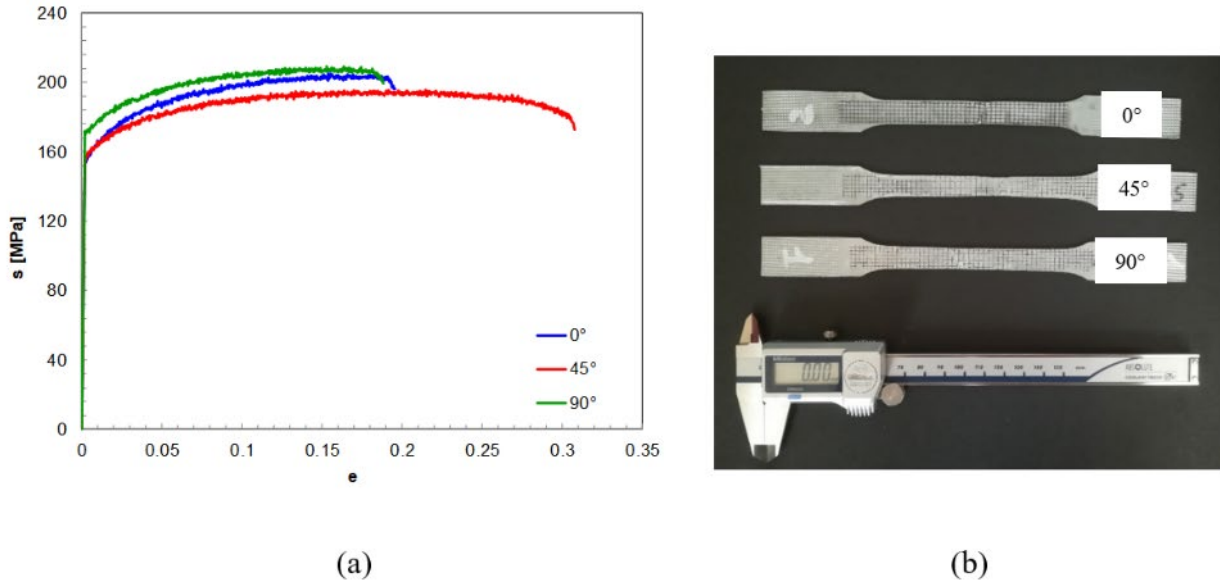

Fig. 8. (a) Effect of the angle of the sample axis with respect to RD on the typical nominal stress vs. nominal strain curves of MPM sandwich, and (b) fractured tension tested samples.

The highest values of yield strength and ultimate tensile strength occur in the transverse direction (Fig. 9a) whilst the longitudinal direction exhibits YS and UTS values similar to the ones obtained along the 45° direction.

Fig. 9b shows that the 0° and 90° directions are characterized by very similar ultimate elongation values. In the 45° angular orientation, the MPM composite exhibits the highest e_t value with a post-necking deformation equal to about 35.3% of the ultimate elongation. In the longitudinal and transverse directions, the post-necking deformation is about 10.4 and 17.1%, respectively, of the e_t value.

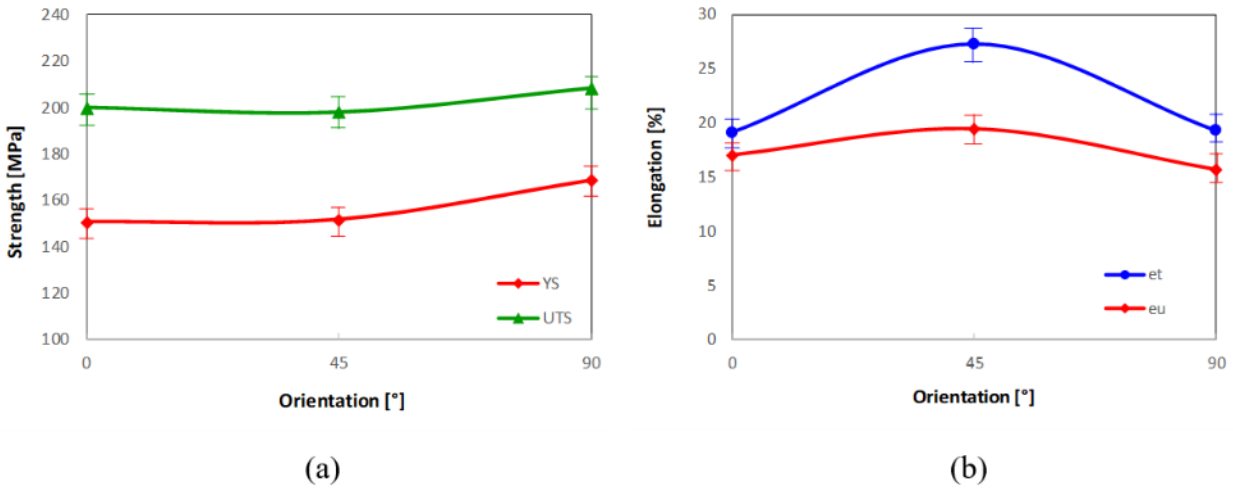

(a) (b)

Fig. 9. Effect of the angle of the sample axis with respect to RD on the: (a) ultimate tensile strength and yield strength, and (b) total uniform elongation and ultimate elongation of MPM sandwich composite.

Fig. 10 shows the true stress vs. true strain curves as a function of the angle of the sample axis with respect to the rolling direction. By plotting σ - ε curves on a log-log scale, the strain hardening exponent values were evaluated [25]. To this purpose, Fig. 11 shows the Hollomon strain-hardening exponent (n) of the MPM sandwich composite vs. the angular orientation. The n value increases with increasing angular orientation of the tensile sample from 0° to 45°; then, the strain-hardening exponent value decreases as the angular orientation is equal to 90°. Such behaviour is very similar to the one exhibited by the strain to the onset of necking (e_t) shown in Fig. 9b. As a matter of fact, the true tensile strength corresponding to the UTS in the s-e plot is reached as the stress increase rate, directly related to the n value, is lower than the rate of area shrinkage in the necking zone. According to Considère criterion [29], at the onset of localized necking, the true strain (at maximum force) is equal to the strain hardening exponent ($\varepsilon_u = n$).

As reported by Hortigón et al. in [30], low n values provide a strain hardening rate that is initially high, but then rapidly decreases with increasing strain. In this case, the material can easily undergo necking as geometrical or microstructural inhomogeneities are present. On the other hand, with high n values, the initial strain hardening is less rapid but continues to high strains; as a consequence, the incipient necking areas harden, thereby preventing further shrinkage and extending the uniform strain behaviour to higher strain values.

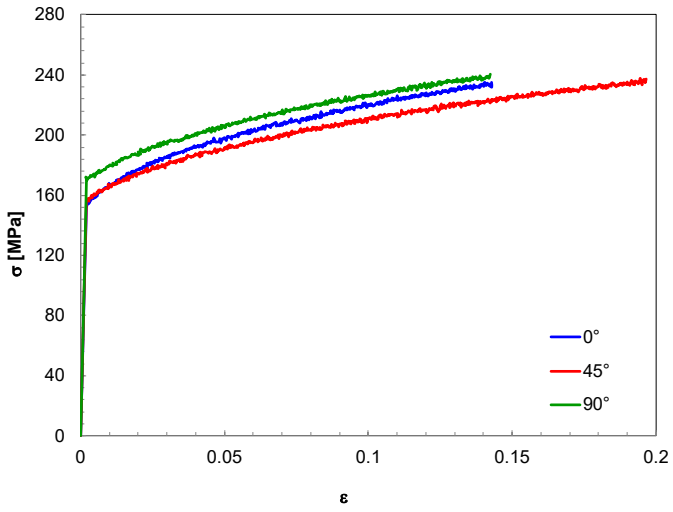

Fig. 10. Influence of the angle of the sample axis with respect to RD on the typical true stress vs. true strain curves until the onset of necking of MPM sandwich composite.

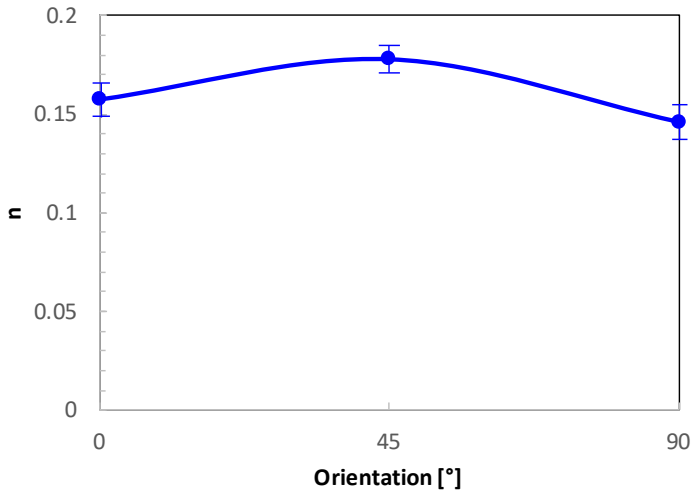

Fig. 11. Influence of the angle of the sample axis with respect to RD on the Hollomon strain hardening exponent of MPM sandwich composite.

As far as the tensile behavior of the steel sheets is concerned, Fig. 12 shows typical nominal stress vs. nominal strain curves until fracture (Fig. 12a) and true stress vs. true strain curves until the onset of necking (Fig. 12b) of HX220Y steel at different angular orientations with respect to the rolling directions.

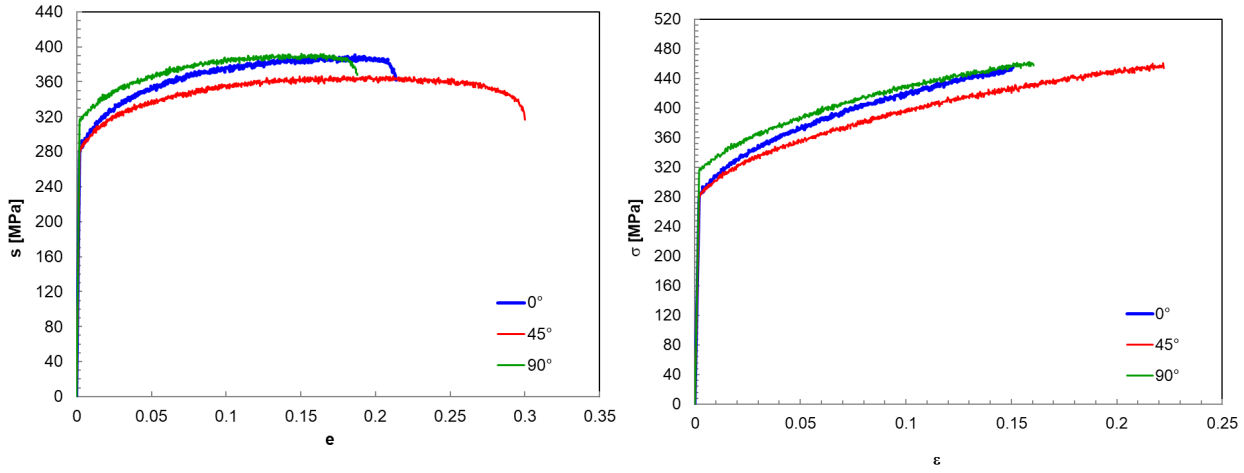

(a) (b)

Fig. 12. Typical (a) nominal stress vs. nominal strain and (b) true stress vs. true strain curves of HX220Y steel at different angular orientations with respect to the rolling directions.

Irrespective of the angular orientations with respect to RD, the mechanical behavior exhibited by the constituent steel is very similar to the one shown by the MPM sandwich composite, even though the cover steel is characterized by higher tensile stress levels and, consequently, higher YS and UTS values than those measured on MPM sandwich composites (Fig.s 8 and 10). No significant variation in the total uniform elongation and ultimate elongation in percentage was found; such result proves that the tensile behavior of the MPM sandwich composite is mainly affected by the cover steel sheet and is in a excellent agreement with those observed by M. Harhash et al. on steel-polymer-steel sandwiches with different sheet and polymer core thicknesses [11]. Also the strain hardening exponent of HX220Y steel (n_{HX220Y}) is higher than the n value of MPM composite (n_{MPM}), as shown by Figure 13. Furthermore, the n_{HX220Y} value is characterized by the same trend of the n_{MPM} one. Such result can be attributed to the soft polymer core which negatively affects the strengthening behavior of the sandwich composites, as also reported by Harhash et al. on sandwich structures composed of cover sheets in low carbon austenitic stainless steel 316L and a core in a commercial polypropylene–polyethylene copolymer foil [13].

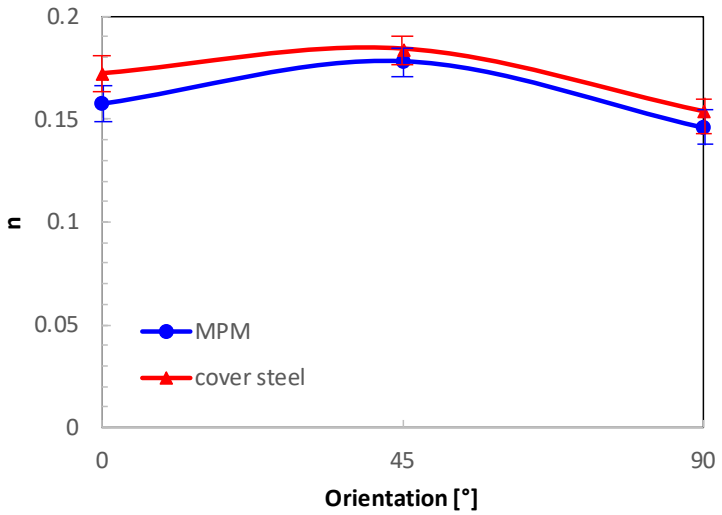

Fig. 13. Comparison between the Hollomon strain hardening exponent of the cover steel and MPM sandwich composite at different angle of the sample axis with respect to RD.

The experimental results on the mechanical properties meet the rule of mixture (ROM) for composite materials, which correlates the properties of the MPM sandwich composite with those of the constituent materials as follows:

$$X_{MPM} \cdot f_{MPM} = X_{cover\ steel} \cdot f_{cover\ steel} + X_{polymer\ core} \cdot f_{polymer\ core} \quad (4)$$

where X_{MPM}, $X_{cover\ steel}$ and $X_{polymer\ core}$ represent a specific property, such as UTS and YS, of MPM, cover steel and polymer core, respectively, whereas f_{MPM}, $f_{cover\ steel}$ and $f_{polymer\ core}$ refers to the volume fractions of the sandwich composite and its constituent materials.

According to the data available in literature on polypropylene–polyethylene polymer [11], the predicted YS and UTS values of the MPM sandwich composite provided by the equation (4) differ on average by 1.9% and 2.1%, respectively, as compared to the experimental ones. Such results denote the excellent agreement between the experimentally measured mechanical properties of the MPM composite and predicted ones using the ROM (Fig. 14).

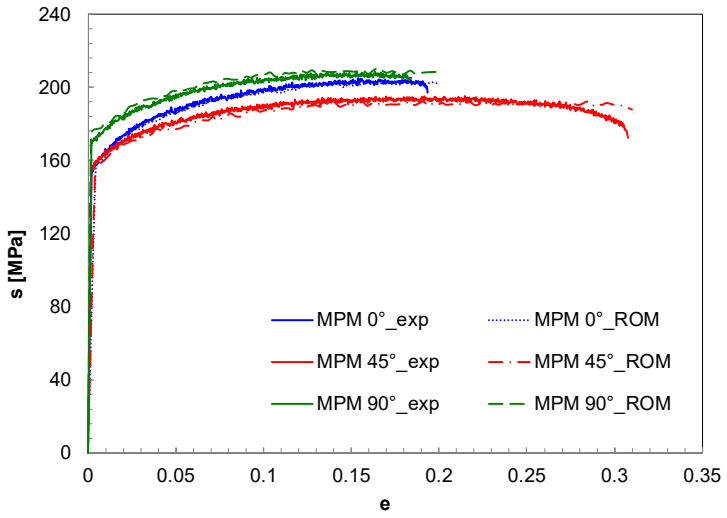

Fig. 14. Comparison between the experimental nominal stress vs. nominal strain curves of MPM sandwich composite at different angular orientations and predicted ones using rule of mixture.

In order to evaluate the anisotropy of the MPM sandwich composite, the experimental results given by tensile tests interrupted in the field of uniform deformation were analyzed. The values of normal anisotropy as a function of the angle of the sample axis with respect to the RD (R_0, R_{45} and R_{90}), average normal anisotropy ($\overline{R}$) and planar anisotropy (ΔR), calculated according to equations (1) – (3), are summarized in Table 1. As a comparison, Table 1 also shows the normal and planar anisotropy values of cover steel sheets.

Table 1. Normal and planar anisotropy values of MPM sandwich composite and HX220Y steel sheet.

	R			ΔR	$\overline{R}$
	R_0	R_{45}	R_{90}		
MPM sandwich	1.48	1.76	1.55	-0.12	1.64
Cover steel sheet	1.50	1.79	1.58	-0.13	1.67

The R values, irrespective of the angular orientation, are higher than 1, indicating that both sandwich composite and cover steel sheet exhibit normal anisotropy, with a reduced attitude to thinning, and very low planar anisotropy, with a low tendency to develop earrings. Furthermore, it can be observed that anisotropy values of the MPM composites are slightly lower than those obtained on constituent steel. Such behavior can be attributed to the higher strain in the thickness of the MPM composite, caused by the contribution of the polymer core, as compared to the strain in the width direction of equation (1).

The mechanical behavior of MPM sandwich composite is consistent with the fracture mechanisms exhibited by tensile tested samples. To this purpose, Fig. 15 shows the SEM images of the fracture surface of a sample with an axis angle equal to 0° with respect to RD. The steel sheets exhibit ductile fracture with nucleation, growth and coalescence of microvoids (Fig. 15a); as they join together and enlarge to the area close to the sample surface, shear fracture occurs. Furthermore, the interface between steel sheet and plastic core fails due to the occurrence of debonding in the regions of higher strain concentration (Fig. 15b). Such behavior is very similar to the one shown by the fractured surfaces at 90° to RD.

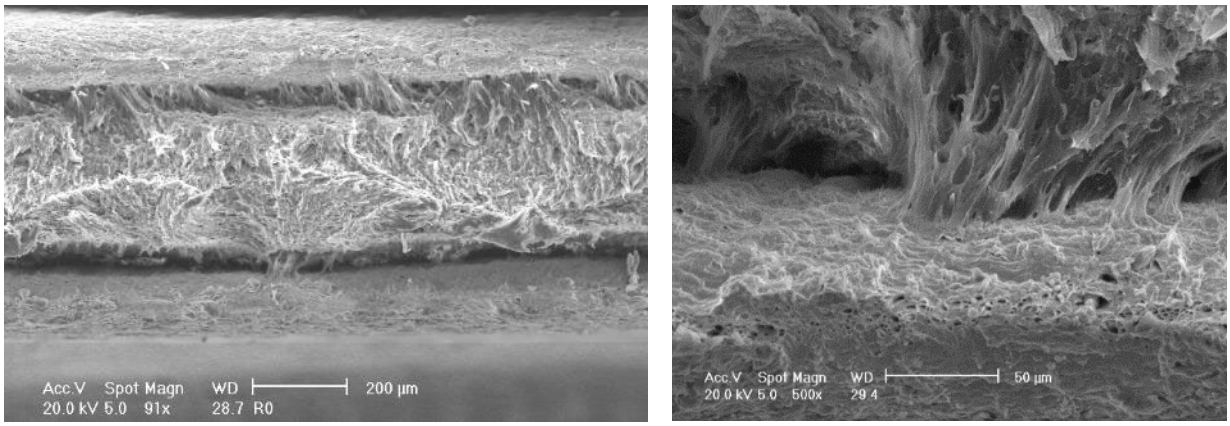

(a) (b)

Fig. 15. SEM micrographs of fractured tensile sample in MPM composite at 0° angular orientation with respect to RD: (a) fracture surface showing the three different layers of the sandwich, and (b) high magnification of the metal-polymer interface.

The SEM micrographs of the fracture surfaces at 45° to RD are shown in Fig. 16. Ductile fracture of the steel layers is still seen whilst the debonding at the metal-polymer interface is less evident as compared with that occurring in the 0° and 90° directions.

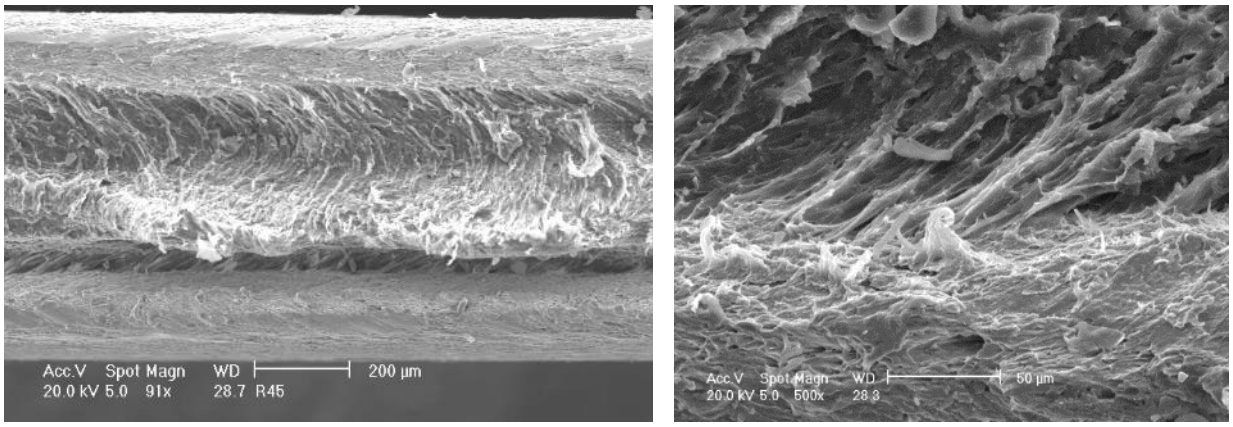

(a) (b)

Fig. 16. SEM micrographs of fractured tensile sample in MPM composite at 45° angular orientation with respect to RD: (a) fracture surface showing the three different layers of the sandwich, and (b) high magnification of the metal-polymer interface.

3.2 Formability

Formability of the metal-polymer-metal sandwich composite was evaluated both in terms of limiting dome height and forming limit curves. By analyzing the punch load vs. punch stroke data recorded during the hemispherical punch test of the disk-shaped sample, the LDH was measured as the stroke at the peak value of punch load. The load-stroke curves obtained by testing several samples are almost coincident providing the excellent repeatability of tests (Fig. 17); furthermore, the high LDH obtained, whose mean value is equal to about 6.3 mm, indicates the very good formability of the MPM sandwich.

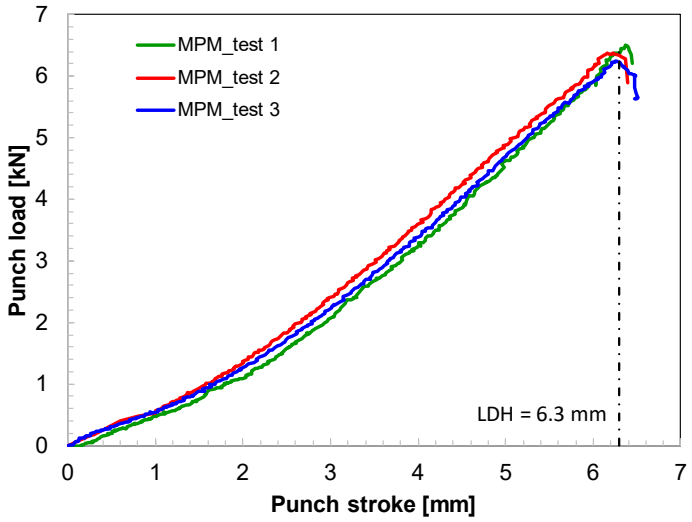

Fig. 17. Punch load vs. punch stroke curves recorded during the hemispherical punch test of disk-shaped samples.

The comparison between punch load vs. punch stroke curves of disk-shaped samples in MPM sandwich composite and cover steel sheet shows that the cover steel sheet exhibits a higher limiting dome height (LDH_{steel} = 6.7 mm) than that reached by MPM sample (LDH_{MPM} = 6.3 mm).

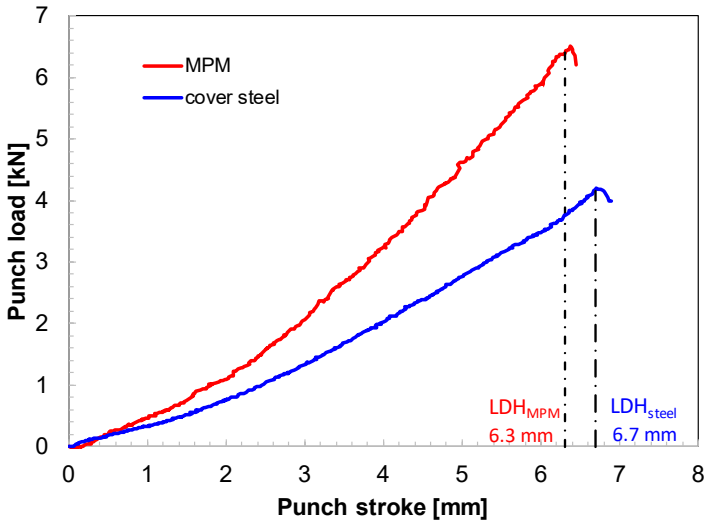

Fig. 18. Comparison between typical punch load vs. punch stroke curves of deformed disk-shaped samples in MPM sandwich composite and cover steel sheets by hemispherical punch tests.

Failure by cracking occurs immediately after the peak of the curves of Fig.s 17 and 18, at the punch rounding near to the top of the dome. In the cover steel sample, crack propagates from the outer surface to the inner one (Fig. 19). On the contrary, the MPM sandwich composite exhibits a surface fracture taking place in the outer skin (Fig. 4b), since the soft polymer core in polypropylene-polyethylene contributes to avoid further crack propagation in the inner skin, as shown by the SEM fractography of Fig. 20 of the outer skin of the MPM disk-shaped sample.

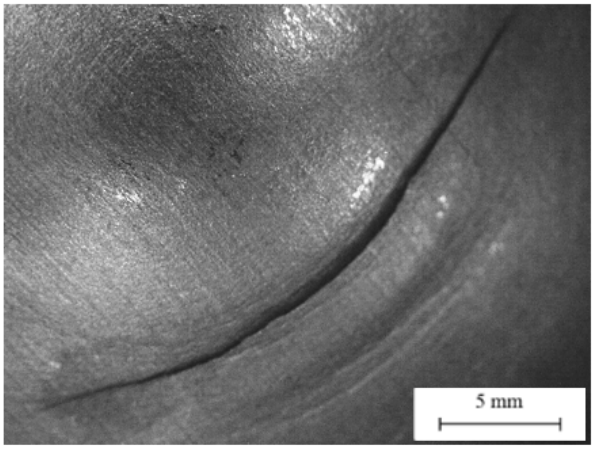

Fig. 19. Typical fracture surface of a disk-shaped sample in cover steel sheet at the onset of failure.

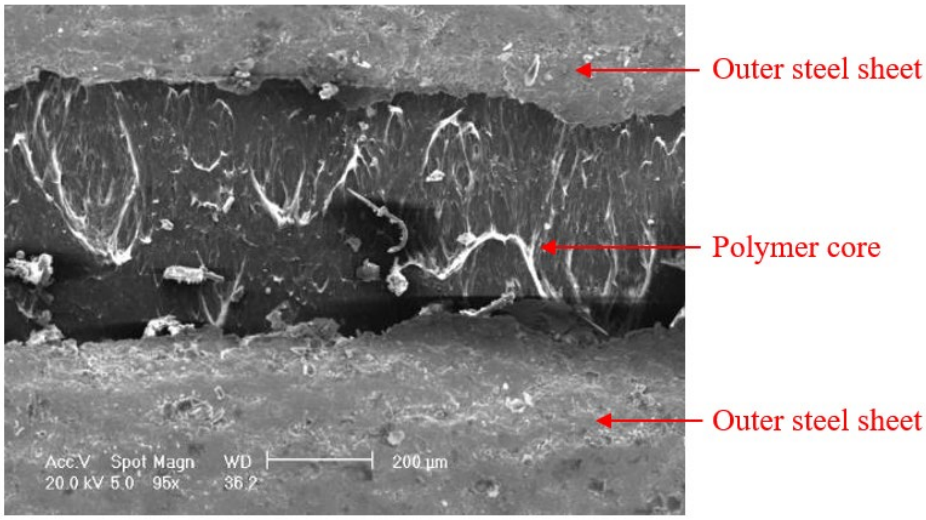

Fig. 20. SEM fractography of the outer skin of the disk-shaped sample immediately after the peak value in the punch load vs. punch stroke curve.

Thicknesses of the three different layers of MPM sandwich composite were measured on the radial cross-section of the deformed disks at 0°, 45° and 90° to RD. The typical half cross-sectional view shown in Fig. 21 highlights the non-uniform deformation along the radial axis.

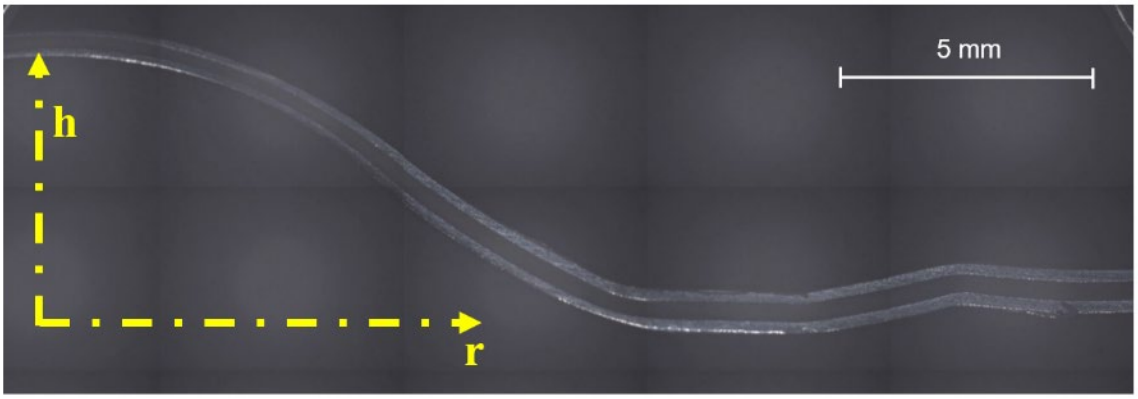

Fig. 21. Half radial cross-section of the disk-shaped sample (orientation: 45° to RD; punch stroke: 6 mm).

Fig. 22 shows the thickness variation of each layer measured in the different zones of the deformed disk-shaped sample as a function of punch stroke and angular orientation with respect to RD. Irrespective of punch stroke and angular orientation, in the flange zone the different layers exhibit a negligible variation or a slight increase in thickness. A marked thinning can be observed from the die edge to the top of the dome, as a result of the balanced biaxial stretching at which disk-shaped sample is subjected during the hemispherical punch test [25]. The metal skins undergo similar thickness reductions even though the outer layer is subjected to a slightly marked thinning than the inner one, according to the results shown by Harhash et al. in [11]. The polymer core is characterized by the highest thickness reduction.

Fig. 22 also shows the effect of punch stroke on the thickness variation as a function of distance from the dome axis. The related data are summarized in Appendix A. As expected, thinning increases with punch stroke, especially near the top of the dome.

As far as the effect of angular orientation with respect to RD on the thickness variation is concerned, at a punch stroke of 5 mm (Fig.s 22a, 22d and 22g), for a given layer, no significant discrepancy in thickness among the different angular orientations appears; at punch strokes of 5.5

and 6 mm, steel skins (Fig.s 22b and 22c, and 22h and 22i) exhibit a thinning along the radial cross-section at 0° and 90° more marked than that observed at 45°, according to the result obtained by tensile tests in terms of both ductility (Fig. 9b) and anisotropy (Table 1). The thickness reduction exhibited by the polymer core does not appear to be significantly affected by the angular orientation with respect to RD (Fig.s 22e and 22f).

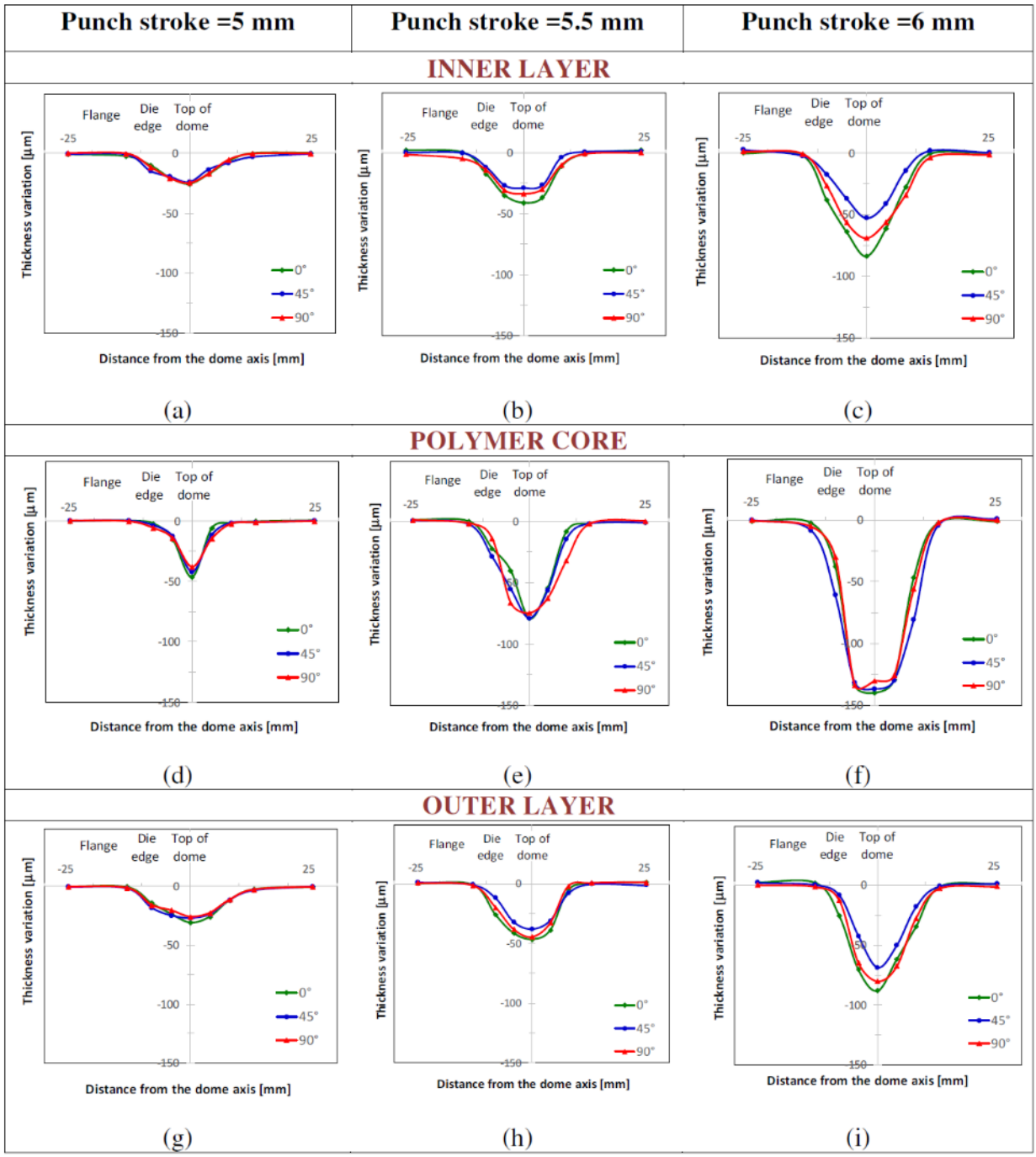

Fig. 22. Effect of punch stroke and angular orientation on the thickness variation measured along the radial cross-section in the different zones of each layer of disk-shaped samples deformed during hemispherical punch test: (a) inner layer, (d) polymer core and (g) outer layer at a punch stroke of 5 mm; (b) inner layer, (e) polymer core and (h) outer layer at a punch stroke of 5.5 mm; (c) inner layer, (f) polymer core and (i) outer layer at a punch stroke of 6 mm.

The forming limit curves, representing the straining conditions below which failure is not yet occurred [25,28], were obtained by subjecting samples with the geometries shown in Fig. 5 to hemispherical punch test.

Fig. 23 shows typical results of the strain measurements on the deformed surface at the onset of failure of a disk-shaped sample, in terms of strain contour maps, obtained by means of the optical grid method. The major and minor strains, acquired from the deformed samples, were plotted in order to obtain the forming limit curves at different angular orientations.

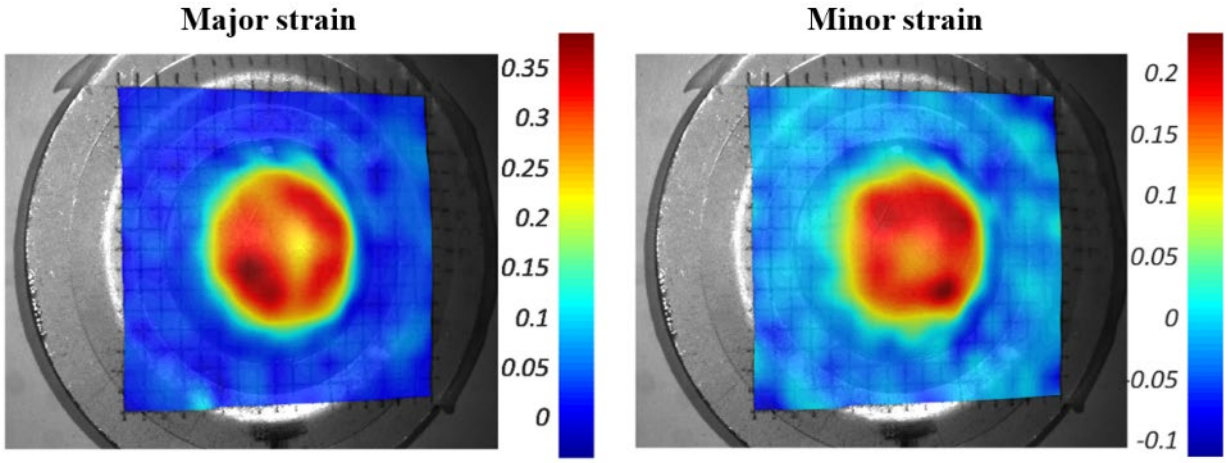

Fig. 23. Typical strain distributions acquired by analyzing the deformation of the regular grid pattern on disk-shaped sample deformed at the onset of failure.

The forming limit curve obtained using samples oriented at 0° to RD is shown in Fig. 24. In the left branch, between uniaxial tension and plane strain conditions, the FLC shows the typical behavior exhibited by metal sheets, with $\varepsilon_2=-\varepsilon_1/2$ in the uniaxial tension condition and $\varepsilon_2=0$ in the plane strain one. Furthermore, the value of FLC at the plane strain condition (FLC_0) is consistent with that obtained by the empirical relationship between FLC_0 and strain hardening exponent defined by Keeler and Brazier [31]:

$$FLC_0 = (0.233 + 0.143 \cdot t) \cdot \frac{n}{0.21} \quad (5)$$

where t is the sheet thickness, in mm, and n the strain hardening exponent. As a matter of fact, by considering t = 0.8 mm and n = 0.161 (Fig. 11) for the 0°angular orientation to RD, a FLC_0 value of 0.266 is obtained, 3.27% lower than the experimental FLC_0 one.

In the right branch of FLC, from plane strain condition to biaxial balanced stretching one, the trend slightly differs from the one typically exhibited by metal sheets. In the biaxial balanced stretching condition, the MPM sandwich composite reaches major strain values higher than the minor ones. Such behavior is in very good agreement with the one obtained by Harhash et al. for the deep-drawable steel grade TS245 sheet and the TS245/PP-PE/TS245 laminate with similar thickness [32].

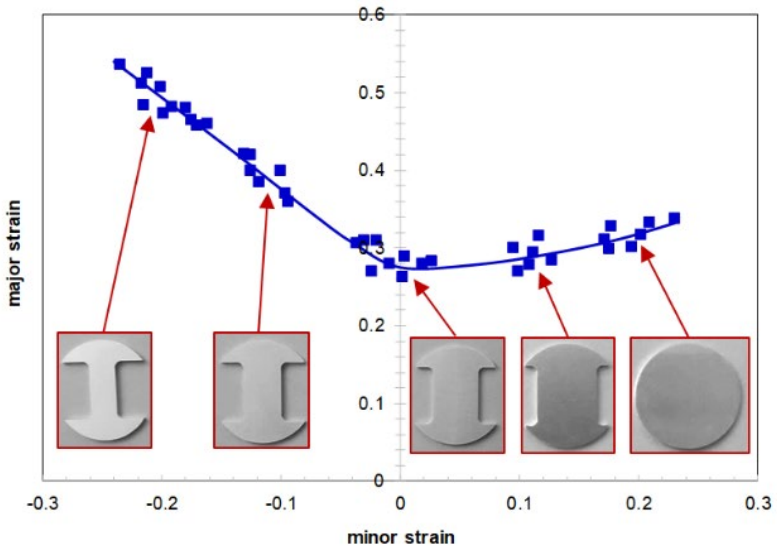

Fig. 24. Forming limit curve of metal-polymer-metal sandwich composite oriented at 0° to RD.

The effect of the angular orientation with respect to the rolling direction on the forming limit curves of MPM sandwich composite is shown in Fig. 25. No appreciable influence of angular orientation on formability is observed in the balanced biaxial stretching condition due to the disk-shaped geometry sample. The angular orientation affects formability in the plane strain and drawing zones. In particular, for a given minor strain, the major strain measured on the samples at 45° to RD is systematically higher than the one at 0°. As far as the samples oriented at 90° are concerned, it appears that the FLC in the drawing region is in between the curves obtained with samples oriented at 0 and 45°. The higher vertical position experienced along 45° angular orientation indicates that,

in the drawing region, such direction is characterized by the highest formability. This is consistent with the results provided by tensile tests in terms of both total uniform and ultimate elongations shown in Fig. 9b and can be related to the lowest attitude to thinning owing to the highest normal anisotropy of the MPM sandwich composite occurring in the 45° angular orientation (Table 1).

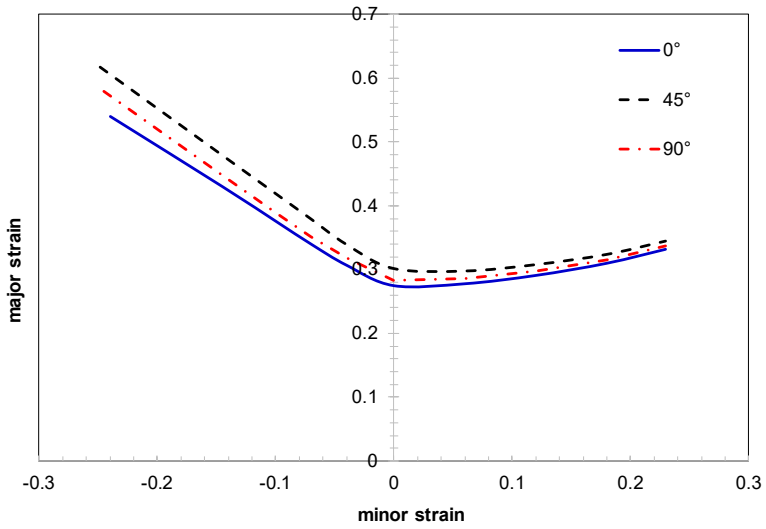

Fig. 25. Effect of the angular orientation with respect to RD on the forming limit curves of MPM sandwich composite.

CONCLUSIONS

Mechanical behavior and formability of metal-polymer-metal sandwich composite, obtained by staking a polymer core film between two steel skins, were investigated by means of uniaxial tensile tests and hemispherical punch tests. The influence of the angular orientation with respect to the rolling direction on strength and forming attitude was analyzed and discussed. The fracture surface of samples was also investigated by the scanning electron microscopy.

The following conclusions can be drawn:

- the nominal stress monotonically rises with nominal strain, in a wide range of uniform deformation;

- the highest ultimate elongation is obtained at 45° to RD, with a wide post-necking deformation. Samples in the 90° angular orientation are characterized by the highest values of yield strength and ultimate tensile strength;
- the highest value of strain-hardening exponent is obtained at 45° to RD;
- the MPM sandwich composite exhibits a normal anisotropy with reduced attitude to thinning and very low planar anisotropy; the highest normal anisotropy value is obtained at 45° to RD.
- a very good formability of the MPM sandwich composite was obtained;
- outer and inner metal skins undergo similar thinning, even though the outer layer is subjected to a slightly marked thickness reduction than the inner one. Polymer core is characterized by the highest thickness reduction;
- thickness reduction increases with punch stroke, especially near the top of the dome;
- at the onset of failure, steel skins exhibit thinning along the radial cross-section at 0° and 90° more marked than that observed at 45°. Thinning in the polymer core is not affected by the angular orientation;
- the influence of angular orientation on formability is negligible in the balanced biaxial stretching condition. The highest vertical position of the forming limit curve, obtained in the 45° orientation to RD in the drawing zone, indicates that formability in such direction is higher than that obtained in the 0° and 90° ones, consistently with the normal anisotropy behavior.

Acknowledgments

The authors wish to thank Massimiliano Pieralisi and Luciano Greco for their support in carrying out the experimental tests.

Author Contributions

Conceptualization, Archimede Forcellese and Michela Simoncini; Data curation, Michela Simoncini; Formal analysis, Archimede Forcellese and Michela Simoncini; Investigation, Michela Simoncini; Methodology, Archimede Forcellese and Michela Simoncini; Project administration,

Archimede Forcellese; Supervision, Archimede Forcellese; Writing – original draft, Michela Simoncini; Writing – review & editing, Archimede Forcellese.

Declaration of Competing Interest.

The authors declare that they have no known competing financial interests or personal relationships that could have appeared to influence the work reported in this paper.

Funding

This research was supported by POR FESR Abruzzo 2014/2020 – Linea di Azione I.1.1 e 1.1.4 – Avviso Pubblico per il "Sostegno a progetti di Ricerca Industriale, Sviluppo Sperimentale e Innovazione delle PMI nelle aree di specializzazione S3" (CUP: C37H18000070007).

Data availability

The experimental results are available upon request.

REFERENCES

[1] Librescu L, Hause T. Recent developments in the modeling and behavior of advanced sandwich constructions : a survey 2000;48:1–17.
[2] Ramnath BV, Alagarraja K, Elanchezhian C. A review on sandwich composite and their applications. Mater Today Proc 2019;16:859–64. https://doi.org/10.1016/j.matpr.2019.05.169.
[3] Alaluss K, Bürkner G. Thermal joining of steel/polymer/steel composite materials using non-direct arcprocess technique. J Manuf Process 2018;34:523–30. https://doi.org/10.1016/j.jmapro.2018.06.032.
[4] Carradò A, Faerber J, Niemeyer S, Ziegmann G, Palkowski H. Metal / polymer / metal hybrid systems : Towards potential formability applications 2011;93:715–21. https://doi.org/10.1016/j.compstruct.2010.07.016.
[5] Huang YM, Leu DK. Finite-element simulation of the bending process of steel/polymer/steel laminate sheets. J Mater Process Tech 1995;52:319–37. https://doi.org/10.1016/0924-0136(94)01617-A.
[6] Tsai SN, Taylor AC. Vibration behaviours of single/multi-debonded curved composite sandwich structures. Compos Struct 2019;226:111291. https://doi.org/10.1016/j.compstruct.2019.111291.
[7] Xie J, Zhang R, Xie G, Manca O. Thermal and thermomechanical performance of actively cooled pyramidal sandwich panels. Int J Therm Sci 2019;139:118–28.

https://doi.org/10.1016/j.ijthermalsci.2019.02.002.
[8] Chatterjee VA, Verma SK, Bhattacharjee D, Biswas I, Neogi S. Enhancement of energy absorption by incorporation of shear thickening fluids in 3D-mat sandwich composite panels upon ballistic impact. Compos Struct 2019;225:111148. https://doi.org/10.1016/j.compstruct.2019.111148.
[9] Colombo C, Harhash M, Palkowski H, Vergani L. Thermographic stepwise assessment of impact damage in sandwich panels. Compos Struct 2018;184:279–87. https://doi.org/10.1016/j.compstruct.2017.10.001.
[10] Mousa S, Kim G. A direct adhesion of metal-polymer-metal sandwich composites by warm roll bonding. J Mater Process Tech 2017;239:133–9. https://doi.org/10.1016/j.jmatprotec.2016.08.017.
[11] Harhash M, Gilbert RR, Hartmann S, Palkowski H. Experimental characterization, analytical and numerical investigations of metal/polymer/metal sandwich composites – Part 1: Deep drawing. Compos Struct 2018;202:1308–21. https://doi.org/10.1016/j.compstruct.2018.06.066.
[12] Kim KJ, Kim D, Choi SH, Chung K, Shin KS, Barlat F, et al. Formability of AA5182/polypropylene/AA5182 sandwich sheets. J Mater Process Technol 2003;139:1–7. https://doi.org/10.1016/S0924-0136(03)00173-0.
[13] Harhash M, Sokolova O, Carradó A, Palkowski H. Mechanical properties and forming behaviour of laminated steel / polymer sandwich systems with local inlays – Part 1. Compos Struct 2014;118:112–20. https://doi.org/10.1016/j.compstruct.2014.07.011.
[14] Ambrogio G, Bruni C, Bruschi S, Filice L, Ghiotti A, Simoncini M. Characterisation of AZ31B magnesium alloy formability in warm forming conditions. Int J Mater Form 2008;1. https://doi.org/10.1007/s12289-008-0027-y.
[15] Forcellese A, Gabrielli F, Simoncini M. Prediction of flow curves and forming limit curves of Mg alloy thin sheets using ANN-based models. Comput Mater Sci 2011;50. https://doi.org/10.1016/j.commatsci.2011.05.048.
[16] Forcellese DA, El Mehtedi M, Simoncini M, Spigarelli S. Formability and microstructure of AZ31 magnesium alloy sheets. vol. 344. 2007. https://doi.org/10.4028/0-87849-437-5.31.
[17] Bruni C, Forcellese A, Gabrielli F, Simoncini M. Modelling of the rheological behaviour of aluminium alloys in multistep hot deformation using the multiple regression analysis and artificial neural network techniques. J Mater Process Technol 2006;177. https://doi.org/10.1016/j.jmatprotec.2006.03.230.
[18] Hussaini SM, Krishna G, Gupta AK, Singh SK. Development of experimental and theoretical forming limit diagrams for warm forming of austenitic stainless steel 316. J Manuf Process 2015;18:151–8. https://doi.org/10.1016/j.jmapro.2015.03.005.
[19] Darabi R, Azodi HD, Bagherzadeh S. Investigation into the effect of material properties and arrangement of each layer on the formability of bimetallic sheets. J Manuf Process 2017;29:133–48. https://doi.org/10.1016/j.jmapro.2017.07.022.
[20] Ruokolainen RB, Sigler DR. The Effect of Adhesion and Tensile Properties on the Formability of Laminated Steels. J Mater Eng Perform 2008;17:330–339.
[21] Stachowiak G, Batchelor AW. Engineering Tribology. Fourth Edi. Elsevier Inc. All; 2014. https://doi.org/https://doi.org/10.1016/C2011-0-07515-4.
[22] Kim L-K, Yu T-X. Forming and failure behaviour of coated, laminated and sandwiched sheet metals: a review. J OfMaterials Process Technol 1997;63:33–42.

[23] Wollmann T, Hahn M, Wiedemann S, Zeiser A, Jaschinski J, Modler N, et al. Thermoplastic fibre metal laminates : Stiffness properties and forming behaviour by means of deep drawing. Arch Civ Mech Eng 2017;18:442–50. https://doi.org/10.1016/j.acme.2017.09.001.
[24] Harhash M, Gilbert RR, Hartmann S, Palkowski H. Experimental characterization, analytical and numerical investigations of metal/polymer/metal sandwich composites – Part 2: Free bending. Compos Struct 2020;232:111421. https://doi.org/10.1016/j.compstruct.2019.111421.
[25] Kalpakjian S, Schmid SR. Manufacturing Engineering & Technology. 8 edition. Pearson; 2019.
[26] International A. ASTM E646-16, Standard Test Method for Tensile Strain-Hardening Exponents (n -Values) of Metallic Sheet Materials, ASTM International, West Conshohocken 2016.
[27] Sasso M, Mancini E, Chiappini G, Simoncini M, Forcellese A. Adapted Nakazima test to evaluate dynamic effect on strain distribution and dome height in balanced biaxial stretching condition. Int J Mech Sci 2018;148:50–63. https://doi.org/10.1016/j.ijmecsci.2018.08.024.
[28] ISO 12004-2:2008 Metallic materials — Sheet and strip — Determination of forming-limit curves — Part 2: Determination of forming-limit curves in the laboratory 2008:27.
[29] Considère M. L'emploi du fer et del´acier dans les constructions. Ann Des Ponts Chaussées 1885:574–775.
[30] Hortigón B, Gallardo JM, Nieto-garcía EJ, López JA. Strain hardening exponent and strain at maximum stress : Steel rebar case 2019;196:175–84. https://doi.org/10.1016/j.conbuildmat.2018.11.082.
[31] Keeler S, Brazier W. Relationships between laboratory material characterization and press shop formability. Int Symp High Strength Low Alloy Steels 1977:517–30.
[32] Harhash M, Carradò A, Palkowski H. Mechanical properties and forming behaviour of laminated steel / polymer sandwich systems with local inlays – Part 2 : Stretching and deep drawing. Compos Struct 2017;160:1084–94. https://doi.org/10.1016/j.compstruct.2016.10.111.

Appendix A

Thickness values and thickness variation measured along the radial cross-section in the different zones of each layer of disk-shaped samples deformed during hemispherical punch test

Punch stroke = 5 mm								
Angular orientation	Zone of the sample	Distance from dome axis [mm]	Thickness [µm]			Thickness variation [µm]		
			inner layer	polymer core	outer layer	inner layer	polymer core	outer layer
0°	Flange	-2.5	198.97	400.10	199.94	-1.03	0.10	-0.06
		-1.3	197.51	400.30	199.64	-2.49	0.30	-0.36
	Die edge	-0.8	189.95	398.06	186.00	-10.05	-1.94	-14.00
		-0.4	179.66	385.20	176.90	-20.34	-14.80	-23.11
	Top of the dome	0	174.60	353.93	169.27	-25.40	-46.07	-30.73
	Die edge	0.4	182.66	394.06	174.35	-17.34	-5.94	-25.65
		0.8	192.95	398.41	188.35	-7.05	-1.59	-11.65
	Flange	1.3	199.85	399.74	197.65	-0.15	-0.26	-2.35
		2.5	200.20	400.59	199.67	0.20	0.59	-0.33
45°	Flange	-2.5	199.65	400.16	199.48	-0.35	0.16	-0.52
		-1.3	199.03	400.12	198.25	-0.97	0.12	-1.75
	Die edge	-0.8	185.30	396.41	182.12	-14.70	-3.59	-17.88
		-0.4	180.45	387.34	175.24	-19.55	-12.66	-24.76
	Top of the dome	0	175.96	358.12	173.00	-24.04	-41.88	-27.00
	Die edge	0.4	186.54	388.47	176.35	-13.46	-11.53	-23.65
		0.8	192.00	398.41	188.45	-8.00	-1.59	-11.55
	Flange	1.3	197.00	398.99	196.57	-3.00	-1.01	-3.43
		2.5	199.86	400.12	199.86	-0.14	0.12	-0.14
90°	Flange	-2.5	200.06	400.18	199.67	0.06	0.18	-0.33
		-1.3	199.64	399.68	198.59	-0.36	-0.32	-1.41
	Die edge	-0.8	188.62	394.18	184.25	-11.38	-5.82	-15.75
		-0.4	179.34	385.69	179.65	-20.66	-14.31	-20.35
	Top of the dome	0	175.29	362.14	174.25	-24.71	-37.86	-25.75
	Die edge	0.4	183.24	385.24	177.49	-16.76	-14.76	-22.51
		0.8	194.29	397.59	188.54	-5.71	-2.41	-11.46
	Flange	1.3	199.47	399.04	197.28	-0.53	-0.96	-2.72
		2.5	199.69	399.74	199.59	-0.31	-0.26	-0.41

Punch stroke = 5.5 mm								
Angular orientation	Zone of the sample	Distance from dome axis [mm]	Thickness [μm]			Thickness variation [μm]		
			inner layer	polymer core	outer layer	inner layer	polymer core	outer layer
0°	Flange	-2.5	201.93	401.46	200.59	1.93	1.46	0.59
		-1.3	200.10	400.26	199.58	0.10	0.26	-0.42
	Die edge	-0.8	182.49	378.21	174.20	-17.51	-21.79	-25.80
		-0.4	165.04	360.20	158.60	-34.96	-39.80	-41.40
	Top of the dome	0	159.14	321.00	153.43	-40.86	-79.00	-46.57
	Die edge	0.4	163.46	346.00	161.04	-36.54	-54.00	-38.96
		0.8	188.68	392.06	195.80	-11.32	-7.94	-4.20
	Flange	1.3	198.69	398.62	200.59	-1.31	-1.38	0.59
		2.5	201.93	399.68	201.59	1.93	-0.32	1.59
45°	Flange	-2.5	199.91	401.06	201.29	-0.09	1.06	1.29
		-1.3	199.51	397.89	199.34	-0.49	-2.11	-0.66
	Die edge	-0.8	188.06	371.59	188.05	-11.94	-28.41	-11.95
		-0.4	173.04	345.18	168.00	-26.96	-54.82	-32.00
	Top of the dome	0	171.08	321.27	162.13	-28.92	-78.73	-37.87
	Die edge	0.4	173.50	344.07	169.06	-26.50	-55.94	-30.94
		0.8	196.12	386.08	192.02	-3.88	-13.92	-7.98
	Flange	1.3	200.51	398.59	199.86	0.51	-1.41	-0.14
		2.5	200.96	399.27	198.69	0.96	-0.73	-1.31
90°	Flange	-2.5	198.69	401.32	200.65	-1.31	1.32	0.65
		-1.3	195.14	398.68	198.44	-4.86	-1.32	-1.56
	Die edge	-0.8	185.78	386.61	180.19	-14.22	-13.40	-19.82
		-0.4	169.01	334.23	162.21	-30.99	-65.77	-37.79
	Top of the dome	0	166.34	325.76	155.72	-33.66	-74.24	-44.28
	Die edge	0.4	170.40	337.85	167.23	-29.60	-62.15	-32.77
		0.8	190.06	368.36	198.17	-9.94	-31.64	-1.83
	Flange	1.3	199.14	398.32	200.65	-0.86	-1.68	0.65
		2.5	199.99	400.63	201.07	-0.01	0.63	1.07

Punch stroke = 6 mm								
Angular orientation	Zone of the sample	Distance from dome axis [mm]	Thickness [μm]			Thickness variation [μm]		
			inner layer	polymer core	outer layer	inner layer	polymer core	outer layer
0°	Flange	-2.5	199.99	398.84	202.16	-0.01	-1.16	2.16
		-1.3	198.51	397.53	201.78	-1.49	-2.47	1.78
	Die edge	-0.8	161.82	362.12	174.26	-38.18	-37.88	-25.74
		-0.4	136.07	266.58	129.32	-63.93	-133.42	-70.68
	Top of the dome	0	116.18	260.14	111.86	-83.82	-139.86	-88.14
	Die edge	0.4	138.63	270.58	138.08	-61.37	-129.42	-61.92
		0.8	172.17	353.12	165.24	-27.83	-46.88	-34.76
	Flange	1.3	199.47	397.56	198.62	-0.53	-2.44	-1.38
		2.5	199.86	398.64	201.08	-0.14	-1.36	1.08
45°	Flange	-2.5	202.78	399.88	201.99	2.78	-0.12	1.99
		-1.3	197.84	391.52	200.25	-2.16	-8.48	0.25
	Die edge	-0.8	182.67	339.15	191.64	-17.33	-60.85	-8.36
		-0.4	162.86	267.85	157.37	-37.14	-132.15	-42.63
	Top of the dome	0	147.04	263.14	131.01	-52.96	-136.86	-68.99
	Die edge	0.4	158.86	269.85	149.37	-41.14	-130.15	-50.63
		0.8	185.67	319.15	181.64	-14.33	-80.85	-18.36
	Flange	1.3	201.78	395.52	198.99	1.78	-4.48	-1.01
		2.5	200.37	400.83	201.27	0.37	0.83	1.27
90°	Flange	-2.5	201.04	399.64	200.12	1.04	-0.36	0.12
		-1.3	199.34	395.08	198.48	-0.66	-4.92	-1.52
	Die edge	-0.8	173.13	370.35	187.16	-26.87	-29.65	-12.85
		-0.4	143.57	266.07	135.42	-56.43	-133.93	-64.58
	Top of the dome	0	130.76	269.62	119.93	-69.24	-130.38	-80.07
	Die edge	0.4	143.57	274.07	132.20	-56.43	-125.93	-67.80
		0.8	165.53	344.02	172.16	-34.47	-55.98	-27.85
	Flange	1.3	196.04	397.64	197.12	-3.96	-2.36	-2.88
		2.5	198.62	399.75	198.76	-1.38	-0.25	-1.24

Figure Captions

Fig. 1. Different layers of the metal-polymer-metal sandwich composite.

Fig. 2. (a) Tensile sample in metal-polymer-metal composite grasped by the machine head clamps and (b) typical fracture surface of a tensile sample.

Fig. 3. Tensile samples obtained by WJC at different orientations to the rolling direction.

Fig. 4. (a) Tooling used in the hemispherical punch tests and (b) disk-shaped sample at the onset of failure.

Fig. 5. Sample with different geometries used in the hemispherical punch tests to obtain the FLCs.

Fig. 6. Disk-shaped sample with the square grid after the 3D coordinates reconstruction by the stereoscopic algorithm.

Fig. 7. Disk-shaped sample cut along the radial cross-section at 0° with respect to RD and embedded for microstructural analysis.

Fig. 8. (a) Effect of the angle of the sample axis with respect to RD on the typical nominal stress vs. nominal strain curves of MPM sandwich, and (b) fractured tension tested samples.

Fig. 9. Effect of the angle of the sample axis with respect to RD on the: (a) ultimate tensile strength and yield strength, and (b) total uniform elongation and ultimate elongation of MPM sandwich composite.

Fig. 10. Influence of the angle of the sample axis with respect to RD on the typical true stress vs. true strain curves until the onset of necking of MPM sandwich composite.

Fig. 11. Influence of the angle of the sample axis with respect to RD on the on the Hollomon strain hardening exponent of MPM sandwich composite.

Fig. 12. Typical (a) nominal stress vs. nominal strain and (b) true stress vs. true strain curves of cover HX220Y steel at different angular orientations with respect to the rolling directions.

Fig. 13. Comparison between the Hollomon strain hardening exponent of cover steel and MPM sandwich composite at different angle of the sample axis with respect to RD.

Fig. 14. Comparison between the experimental nominal stress vs. nominal strain curves of MPM sandwich composite at different angular orientations and predicted ones using rule of mixture.

Fig. 15. SEM micrographs of fractured tensile sample in MPM composite at 0° angular orientation with respect to RD: (a) fracture surface showing the three different layers of the sandwich, and (b) high magnification of the metal-polymer interface.

Fig. 16. SEM micrographs of fractured tensile sample in MPM composite at 45° angular orientation with respect to RD: (a) fracture surface showing the three different layers of the sandwich, and (b) high magnification of the metal-polymer interface.

Fig. 17. Punch load vs. punch stroke curves recorded during the hemispherical punch test of disk-shaped samples.

Fig. 18. Comparison between typical punch load vs. punch stroke curves of deformed disk-shaped samples in MPM sandwich composite and cover steel sheets by hemispherical punch tests.

Fig. 19. Typical fracture surface of a disk-shaped sample in cover steel sheet at the onset of failure.

Fig. 20. SEM fractography of the outer skin of the disk-shaped sample immediately after the peak value in the punch load vs. punch stroke curve.

Fig. 21. Half radial cross-section of the disk-shaped sample (orientation: 45° to RD; punch stroke: 6 mm).

Fig. 22. Effect of punch stroke and angular orientation on the thickness variation measured along the radial cross-section in the different zones of each layer of disk-shaped samples deformed during hemispherical punch test: (a) inner layer, (d) polymer core and (g) outer layer at a punch

stroke of 5 mm; (b) inner layer, (e) polymer core and (h) outer layer at a punch stroke of 5.5 mm; (c) inner layer, (f) polymer core and (i) outer layer at a punch stroke of 6 mm.

Fig. 23. Typical strain distributions acquired by analyzing the deformation of the regular grid pattern on disk-shaped sample deformed at the onset of failure.

Fig. 24. Forming limit curve of metal-polymer-metal sandwich composite oriented at 0° to RD.

Fig. 25. Effect of the angular orientation with respect to RD on the forming limit curves of MPM sandwich composite.

Table Captions

Table 1. Normal and planar anisotropy values of MPM sandwich composite and HX220Y steel sheet.

Prof. Archimede Forcellese is Full Professor at the School of Engineering of the Polytechnic University of Marche, in which he lectures in graduate courses in Mechanical Engineering. In 2013, he obtained the National Scientific Qualification to cover the position of full professor. His research activity is mainly addressed on: i) metal forming processes of lightweight alloys, such as aluminium and magnesium alloys, and composites; ii) solid state joining processes, such as friction stir welding; iii) machining operations and tool wear mechanisms; iv) design and control of manufacturing processes by means of artificial intelligence techniques; v) sustainable manufacturing.

Prof. Michela Simoncini graduated cum lode in Mechanical Engineering at the Polytechnic University of Marche in 2003, where received her Ph.D. in Mechanical Engineering in 2006. Currently, she is Associate Professor at the School of Engineering of the eCampus University in which she lectures in graduate courses in Industrial Engineering. Her research activity is mainly focused on: i) innovative production processes, with particular reference to processing for plastic deformation, machining and solid state welding processes, applied to advanced materials such as innovative metal lightweight alloys, composites both with a discontinuous and continuous reinforcement phase; ii) sustainable manufacturing using LCA methodology; iii) quality assurance of product/process.